

Oxidation Kinetics and Mechanism of Boron in Metallurgical-Grade Silicon Melt by Oxidizing Refining



QILIANG WANG, NAIYONG HE, JIJUN WU, KUIXIAN WEI, and WENHUI MA

This research paper aims to optimize the purification process of industrial silicon oxygen blowing refining by exploring the reaction mechanism. The objective is to promote the widespread application and further development of photovoltaic technology. The article employs a combination of experimental analysis and *ab initio* molecular dynamics simulation calculations to investigate the oxidation mechanism for the removal of boron from metallurgical-grade silicon. The relationship between refining time and boron concentration in refined silicon was fitted to obtain the apparent rate constant and mass transfer coefficient of boron, which were determined to be 5.68×10^{-4} and $1.37 \times 10^{-5} \text{ m s}^{-1}$. Our experimental findings indicate a significant increase in the rate of silicon loss with prolonged refining time. Furthermore, our *ab initio* molecular dynamics simulation shows a strong interaction between B–O at higher temperatures, highlighting the effectiveness of oxygen blowing in boron removal. Using the Materials Studio software, the mean square displacement of impurity boron in silicon melt was calculated, yielding diffusion coefficients of 6.756×10^{-9} and $9.366 \times 10^{-9} \text{ m}^2 \text{ s}^{-1}$ at temperatures of 1723 K and 1823 K.

<https://doi.org/10.1007/s11663-024-03022-4>

© The Minerals, Metals & Materials Society and ASM International 2024

I. INTRODUCTION

AMONG the materials utilized in the construction of solar cells in the photovoltaic industry,^[1] silicon stands out as the one most commonly used.^[2] Researchers have recognized various approaches to augment the efficiency of silicon-based solar cells, such as modifying the silicon surface and introducing doping materials.^[3] Refining is crucial to minimize impurities and enhance the quality of industrial silicon by reducing impurity contents. Refining technologies for high-quality industrial silicon include blowing refining,^[4,5] slag refining,^[6,7] solvent refining,^[8]

electromagnetic refining,^[9] vacuum refining,^[10] directional solidification,^[11] or a combination of these methods.^[12] The effectiveness of conventional refining methods, such as vacuum refining and directional solidification, in removing boron from silicon is limited due to boron's high partition coefficient and low saturated vapor pressure.^[13] An effective and affordable method to remove impurities including boron, aluminum (Al), calcium (Ca), and titanium (Ti) is air blowing refining.^[14] The main method for refining silicon metal in industrial production is through air blowing. This method effectively reduces the boron impurity content by converting boron impurities into other substances through a chemical reaction with oxygen.^[5]

Oxygen blowing refining is a process of selective oxidation that utilizes the varying oxidizing properties of elements. During the process, the silicon melt is stirred which allows for more free oxygen ions to dissolve in the silicon, leading to complete contact and reaction with impurities. As a result, impurities get enriched and removed from the surface of the silicon solution. The continuous stirring facilitates optimal kinetic conditions, which accelerates the rate of chemical reaction and generates volatile compounds, achieving optimal removal of B. However, the kinetics of deep removal of impurities are limited and can be influenced by the blowing rate, gas type, and gas pressure. Therefore, more research on refining processes and kinetics is necessary, especially in the field of crystalline

QILIANG WANG and KUIXIAN WEI are with the State Key Laboratory of Complex Nonferrous Metal Resources Clean Utilization, Kunming University of Science and Technology, Kunming 650093, P.R. China and also with the Faculty of Metallurgical and Energy Engineering, Kunming University of Science and Technology, Kunming 650093, P.R. China. NAIYONG HE is with the Faculty of Metallurgical and Energy Engineering, Kunming University of Science and Technology. JIJUN WU and WENHUI MA are with the State Key Laboratory of Complex Nonferrous Metal Resources Clean Utilization, Kunming University of Science and Technology and with the Faculty of Metallurgical and Energy Engineering, Kunming University of Science and Technology and also with The National Engineering Laboratory for Vacuum Metallurgy, Kunming University of Science and Technology, Kunming 650093, P.R. China. Contact e-mails: dragon_wu213@126.com; mwhsilicon@126.com

Manuscript submitted May 29, 2023; accepted January 18, 2024.

silicon materials.^[15,16] The presence of H₂O and O₂ in the gas mixture results in the oxidation of boron impurities, producing boron oxides (B_xO_y) and boron hydroxides (H_zB_xO_y).^[17] Thermodynamic calculations indicate that the primary volatiles for boron and silicon are HBO and SiO, respectively, with secondary volatile species including HBO₂, BH_x (x = 1 to 3), and SiH_y (y = 1 to 3).^[15] Under alkaline conditions, H₂O can decompose into (H⁺) and (OH⁻), facilitating the removal of boron by generating gaseous boride HBO with (OH⁻). The study found that the optimal boron removal rate of 96.77 pct was achieved at a volume ratio of H₂O/O₂ of 2, with impurity boron content reaching a minimum value of 0.71 parts per million by weight (ppmw).^[18] Næss *et al.*^[19] conducted a study on the active oxidation rate of silicon melt in a 75 kW induction furnace. They used a lance to blow an oxidizing gas above the surface of the silicon melt and collected the silica formed by the reaction. The study found that the fuming rate was determined by the gas composition and flow rate. The researchers also used computational fluid dynamics and kinetic models to model the system and concluded that the gas flow rate above the silicon melt was the most significant factor affecting the rate of silicon fumigation.

This research paper uses air blowing refining to study the mass transfer of impurity B in silicon melt during the industrial silicon refining process. A kinetic model was developed to explain the oxidation of non-metallic impurities B, providing a theoretical foundation for the kinetics of industrial silicon refining. The objective of this study is to enhance the efficiency of the industrial refining process.

II. EXPERIMENTAL AND SIMULATION CALCULATION

A. Mechanism and Kinetic Derivation of Boron Oxidation Refining

The refining process for metallurgical-grade silicon involves a chemical reaction and transfer of materials between gas and impurities in the silicon melt. This reaction can be divided into the following steps^[4]: (a) diffusion of [M] in the silicon melt and (SiO₂) in the slag towards the interface between the two; (b) once they reach the interface, [M] chemically reacts with (SiO₂); (c) the resulting (MO) and [Si] diffuse towards the slag and silicon melt, respectively. The compositional relationship and concentration distribution of the reaction process between boron and the silicon melt in the purification of metallurgical-grade silicon oxide impurities is shown in Figure 1.

The rate equation for impurity [M] removal in the industrial silicon oxygen blowing refining process is shown in Eq. [1].^[20]

$$\frac{dw[M]}{dt} = -k_M(w[M] - w[M]_{eq}) \quad [1]$$

Equation [2] can be obtained from the integration of Eq. [1].

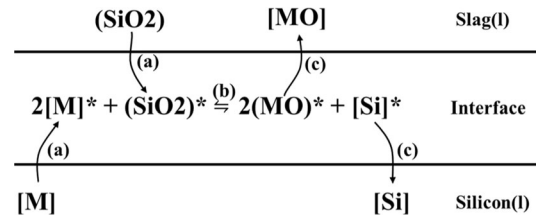


Fig. 1—Action steps between impurity [M] and oxidizing medium in silicon melt.

$$\ln \frac{w[M] - w[M]_{eq}}{w[M]_o - w[M]_{eq}} = -k_M \cdot t \quad [2]$$

where k_M is the apparent rate constant of M. $w[M]$, $w[M]_o$, and $w[M]_{eq}$ are the instantaneous, initial and equilibrium concentrations (wt pct) of M in the silicon solution, respectively. Assuming that [M] in the silicon solution is zero, when the equilibrium is reached, Eq. [3] can be written as follows:

$$\ln \frac{w[M]}{w[M]_o} = -k_M \cdot t \quad [3]$$

The relationship between the apparent rate constant and the mass transfer coefficient is shown in Eq. [4]. Therefore, if the value of $\frac{A}{V}$ is known, the value of β_M can be calculated by Eq. [4].

$$k_M = \beta_M \times \frac{A}{V} \quad [4]$$

where β_M is the mass transfer coefficient of M ($m \text{ s}^{-1}$), and $\frac{A}{V}$ is the interface area per unit volume of the molten slag and silicon melt (m^{-1}).

B. Experimental Method

The experiment utilized industrial silicon from a manufacturer in Yunnan Province, China with 58 ppmw boron content. The argon and oxygen used in the experiment had a purity level of 99.95 pct. Equipment used included a high-temperature gas blowing furnace (16Q-YC), diamond wire cutting machine (SAMICK SK-25), polishing machine (UNIPOL-1502), and vibration mill (ZDM-51ML). Detection instruments included inductive coupled plasma-atomic emission spectrometry (ICP-AES, ELAN DRC).

In this experiment, a powdered industrial silicon sample with a mass of 50 ± 0.01 g was loaded into a 54 mL corundum crucible. Then place the crucible into a magnesium oxide crucible in a resistance furnace, and heat it at a rate of 276 K/min for different times. During the heating process, argon gas was introduced into the furnace to prevent pollution. After reaching different refining temperatures, the Ar–O₂ gas mixture is blown into the furnace through a corundum tube placed one centimeter above the crucible. Different mixed gases were set, and the flow rates of Ar and O₂ were changed. The experimental conditions are as follows Table I. The samples were taken out of the furnace, weighed, and

Table I. Experimental Conditions for Removing Impurity B from Industrial Silicon

Serial Number	Refining Time (min)	Total Gas Flow Rate (mL/min)	Refining Temperature (K)	Gas Composition (mL/min)	
				Ar	O ₂
1	90	400	1723	200	200
2	90	400	1753	200	200
3	90	400	1783	200	200
4	90	400	1823	200	200
5	90	400	1843	200	200
6	90	400	1873	200	200
7	10	600	1823	200	400
8	30	600	1823	200	400
9	50	600	1823	200	400
10	70	600	1823	200	400
11	120	600	1823	200	400
12	90	400	1823	0	400
13	90	400	1823	100	300
14	90	400	1823	300	100

separated by diamond wire cutting. The refined slag was recovered as much as possible and weighed. The samples of refined silicon and slag were determined by ICP-AES.

C. Establishment of Molecular Dynamics Model

While molecular dynamics simulations are primarily employed for the investigation of crystalline structures, their efficacy extends to the study of amorphous materials as well. In simulations concerning amorphous or liquid substances, the constituent atoms or molecules are not confined within a crystal lattice, thus facilitating their freedom of movement. This attribute enables the effective capture of short- and medium-range orderings characteristic of liquids or amorphous substances. To accurately simulate these states, appropriate potential energy functions and initial conditions are selected. The potential energy functions define the interactions among atoms or molecules within the system, and the initial conditions determine the position, velocity, and other parameters of the particles at the onset of the simulation. The accuracy and reliability of these simulation results are often validated by comparing them with experimental data. This comparison assists in assessing the extent to which the simulation accurately replicates the properties and behaviors observed in real-world experiments. In summary, although initially developed for crystalline structures, molecular dynamics simulations have been adeptly adapted for the study of liquid or amorphous substances through the implementation of suitable methodologies and validation techniques. Consequently, we have established a kinetic model for the oxidation of the non-metallic impurity boron, providing a theoretical foundation for the kinetics of industrial silicon refining.

The Cambridge Serial Total Energy Package (CASTEP) employs ultrasoft pseudopotentials to describe atomic interactions and utilizes the generalized gradient approximation for the exchange-correlation functional. To ensure accurate calculations, certain parameters were set. The energy cutoff was set at 300

eV, allowing for the inclusion of a wide range of electronic states. The k-point mesh was set to $3 \times 3 \times 1$, which is a grid used to sample the Brillouin zone in calculations involving periodic systems. The self-consistent process carried out by CASTEP involves iterative calculations to achieve convergence of the system's energy and charge density distribution. A high level of accuracy, better than 2×10^{-6} eV/atom, was targeted for energy convergence during this process. By utilizing CASTEP with these settings can effectively analyze and understand the properties and behavior of materials at the atomic scale.

The choice of grain boundary (GB) plane directions is crucial in studying the properties and behavior of materials. Based on relevant studies cited as References 21, 22, it has been observed that Si (110) and Si (111) are the preferred GB plane directions in silicon. For this particular study, the Si (111) surface was selected as the interaction interface for building a supercell and introducing impurity and oxygen atoms. The Si (111) surface is commonly used in investigations due to its unique crystallographic orientation and surface reactivity. To simulate realistic conditions and explore the reaction mechanism of oxygen purification in industrial silicon, two temperatures were chosen: 1723 K and 1823 K. These temperatures are close to the melting point of silicon and the actual refining temperature. By selecting temperatures in this range, the aim to better understand the purification process and the behavior of oxygen atoms in silicon at elevated temperatures that mimic industrial conditions.

The Si-B supercell was employed as a representation of the silicon melt for the incorporation of oxygen atoms. To obtain the equilibrium structure, the geometry optimization process was performed using the Broyden-Fletcher-Goldfarb-Shanno (BFGS) algorithm, which iteratively adjusts the atomic positions until convergence is achieved. The resulting supercell consists of 137 Si atoms, 5 O atoms, and 2 impurity atoms, making a total of 144 atoms. Subsequently, *ab initio* molecular dynamics simulations were carried

Table II. The Main Impurity Content in MG-Si

Elements	Fe	Al	Ca	Ti	B	P
Content (ppmw)	4600	1400	240	450	58	56

out using the optimized stable structure. The simulations were conducted in the NVT ensemble, which maintains a constant number of particles, volume, and temperature. The Nose temperature control method was utilized to regulate the temperature, with settings of 1723 K and 1823 K. The time step employed was 1 fs, and the simulation time spanned 1 ps. In order to obtain further insights, we start from the chemical composition and crystal structure of the material, and obtain various ground state information of the material by calculation. Among them, the density of states and the density of states can better show the effect of O on the electronic structure and properties of the Si-B superlattice. For this study, the valence electron configurations considered were Si-3s23p2, B-2s22p1, and O-2s22p4, taking into account the electronic structure of the corresponding atoms. The primary focus of this research is to investigate the impact of oxygen doping on the properties of the silicon melt. This is achieved through a combination of theoretical calculations and molecular dynamics simulations, providing valuable insights into the behavior and characteristics of the system under study.

III. RESULTS AND DISCUSSION

A. Impurity Morphology in Silicon After Refining

The raw materials were processed into powder form by using a vibratory mill, and the results were examined by ICP-AES. The results are shown in Table II.

The aim of this research paper is to investigate the removal of impurity B in industrial silicon by blowing Ar-O₂ mixed gas and altering refining temperature, refining time, and gas composition. Based on the data obtained from the experiment, the results in Figure 2 indicate that the B content in industrial silicon is 0.0087 pct after conducting the experiment.

The results of this study indicate that refining temperatures between 1823 K and 1873 K gradually decrease the impurity content in silicon, yet the rate of impurity decrease slowly decreases with increasing temperature. The contact reaction between slag and silicon can promote the conversion of impurity boron, which is more complete at higher temperatures. The highest impurity removal efficiency is achieved at a range of 1753 K to 1823 K. The impurity content changes smoothly until the end after 50 minutes of refining, and the curve gradually flattens, indicating successful impurity removal. A good removal effect of impurity B can be achieved by controlling the O₂ flow rate at 200 mL/min. The impurity B content decreased to 0.0010 pct after refining.

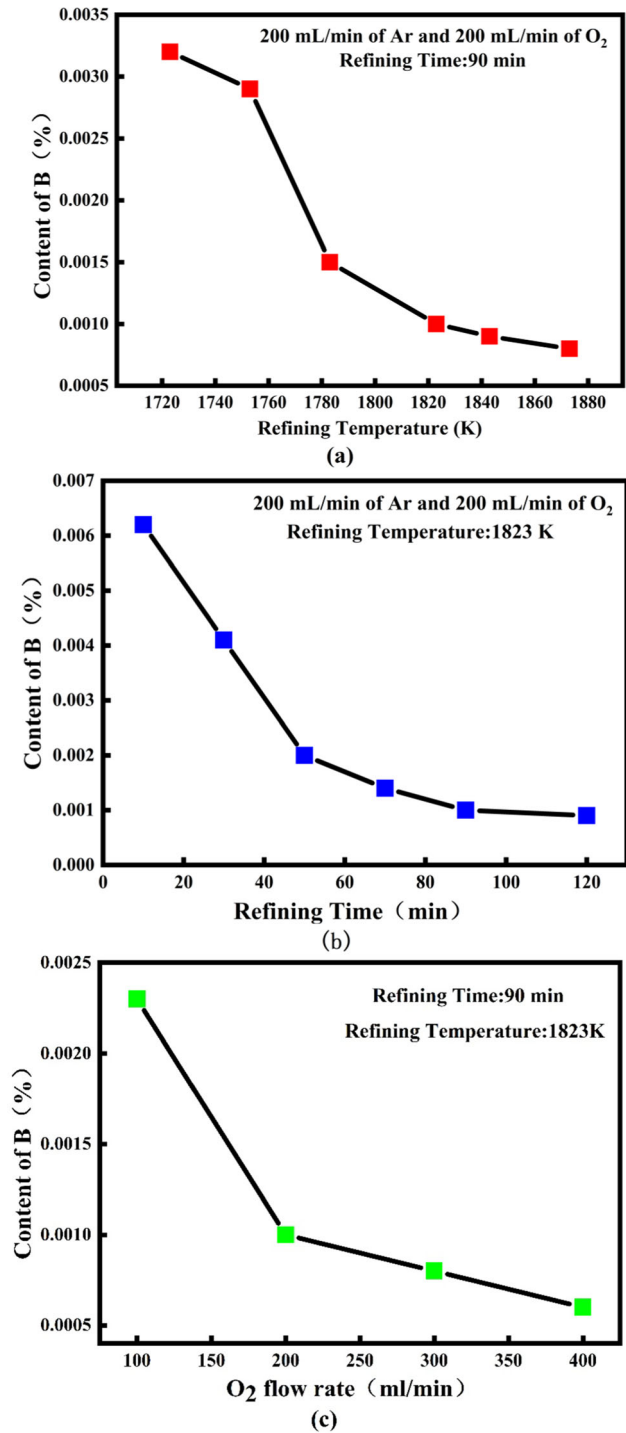


Fig. 2—Content of Impurity B under Different Refining Conditions: (a) refining temperature; (b) refining time; (c) gas flow.

B. Kinetics of Oxidizing Refined Boron

In this experiment, the initial boron content of sample B was 58 parts per million by weight (ppmw). After refining at a temperature of 1550 °C for 90 minutes, the boron content was reduced to 10 ppmw. The corresponding changes in boron content over time for industrial-grade silicon are presented in Figure 3. It is observed that the boron content generally decreases with

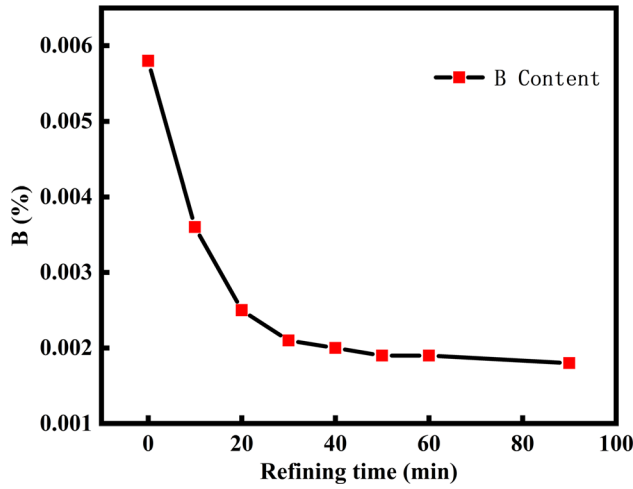


Fig. 3—Effect of refining time on impurity B removal from industrial silicon.

increasing refining time, but the rate of decrease gradually slows down over time. The removal rate of B was faster in the first 30 minutes, after which the content remained relatively stable. The reaction progressed, the impurity content in the silicon melt gradually decreased, the rate-limiting step changed, and the overall reaction rate also changed. Additionally, it is possible that the surface of the silicon melt oxidized and formed a crust at the reaction interface, reducing the effective reaction area and slowing down the reaction rate.

$$\ln \frac{w[B]}{w[B]_0} = -k_B \cdot t \quad [5]$$

According to Eq. [3], the kinetic equation for impurity B removal during the oxygen blowing refining process can be expressed as Eq. [5]. Combining Eq. [5] and experimental results shown in Figure 3, the relationship of $\ln \frac{w[B]}{w[B]_0}$ to t is shown in Figure 4.

As shown in Figure 4, there is a strong linear relationship between the variables $\ln \frac{w[B]}{w[B]_0}$ and t . Thus, Eq. [5] appears to be a suitable rate expression, indicating that the removal reaction is first-order. Based on the slope obtained from Figure 4, we can calculate the apparent rate constant of B (k_B) during the refining process as $5.68 \times 10^{-4} \text{ m s}^{-1}$.

The dimensions of the sample after industrial silicon oxygen blowing refining are shown in Figure 5. The shape of the refined silicon sample is a cylinder, so $\frac{d}{V} = \frac{1}{h}$. During the experiment, the height h of the silicon melt was in dynamic change as the temperature increases and the reaction proceeds. The density at high temperature ($\rho_{Si} = 2470 \text{ kg m}^{-3}$ at $1550 \text{ }^\circ\text{C}$)^[23] was greater than that at room temperature ($\rho_{Si} = 2330 \text{ kg m}^{-3}$ at $25 \text{ }^\circ\text{C}$)^[23] resulted in a decrease in h . In addition, h decreased with the volatilization of silicon. The $\frac{d}{V}$ value of the reaction is reasonably estimated based on the average sample height h after the experiment and considering the slight

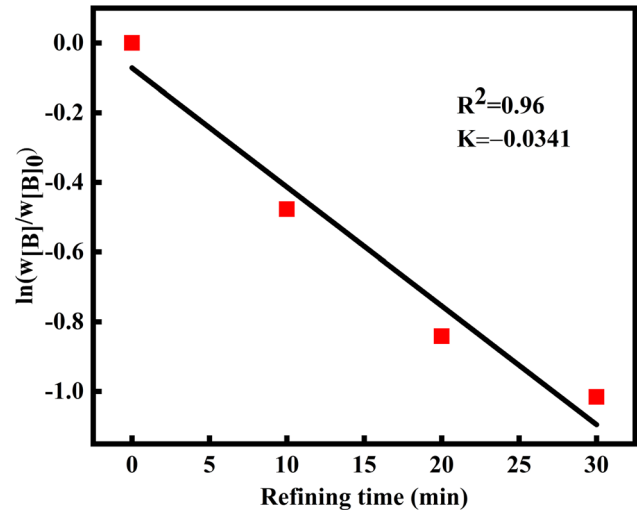


Fig. 4—The relationship between $\ln \frac{w[B]}{w[B]_0}$ and t .

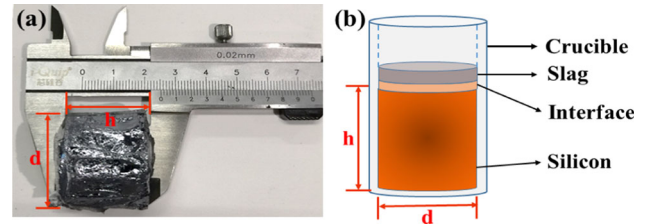


Fig. 5—(a) Schematic diagram of refined silicon sample, (b) crucible size after O_2 blowing refining.

volume reduction after refining. And the value of $\frac{d}{V}$ is obtained as 41.4 m^{-1} . Bringing the value of $\frac{d}{V}$ into Eq. [4], the mass transfer coefficient of impurity B (β_B) in the silicon melt is calculated as $1.37 \times 10^{-5} \text{ m s}^{-1}$. Since the blown-in oxygen has an agitating effect on the molten silicon, it accelerates the diffusion of impurity B in the silicon melt, resulting in a larger mass transfer coefficient.

C. Silicon Loss of Slag Refining Process

During air blowing refinement, some of the silicon is oxidized, leading to a reduction in silicon content. The rate of this loss in silicon can be determined by calculating the difference in weight before and after the refining process. The loss rate of silicon (represented by the symbol η) can be calculated using Eq. [6].

$$\eta = \frac{m - m_m}{m} \times 100 \text{ pct} \quad [6]$$

where η (pct) is the silicon loss rate; m (g) is the quality of the raw material; m_m (g) is the mass of the silicon after refining.

The data for the silicon samples before and after refining are compiled as shown in Table III.

Table III. Oxidization and Mass Loss of Silicon Before and After Oxygen Blowing Refining

Serial Number	Raw Material m (g)	Blowing Time t (minutes)	Silicon Quality After Refining m_m (g)	Silicon Loss Rate η (Pct)
1	50.01	10	49.16	1.68
2	50.01	20	48.42	3.16
3	50.01	30	47.39	5.22
4	50.01	40	46.75	6.51
5	50.01	50	46.39	7.22
6	50.01	60	45.91	8.18
7	50.01	90	44.94	10.12

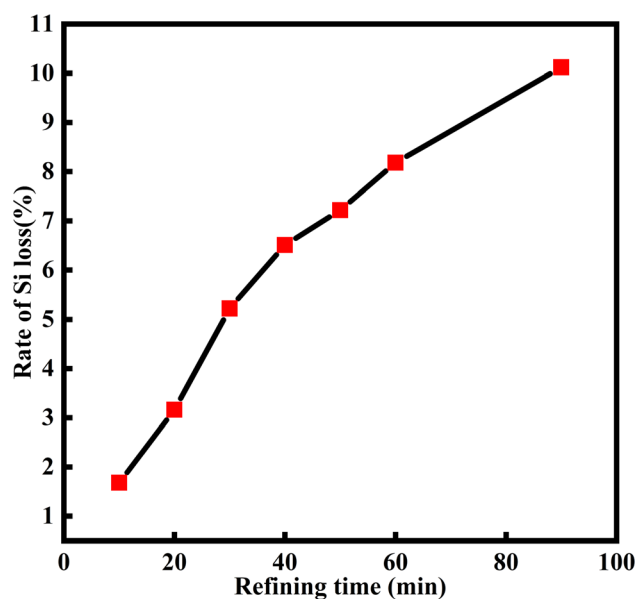


Fig. 6—Relationship between silicon loss rate and refining time.

Based on the experimental data presented in Table III, it is evident that there is a direct relationship between the refining time and silicon loss rate, as illustrated in Figure 6. The data shows that the silicon loss rate gradually rises as the refining time increases, culminating in reaching its peak value of 10.12 pct at 90 minutes.

During the refining process, silicon in the melt is oxidized to silicon oxides, which, along with impurity oxides, form a slag system. The slag-silicon interface results in the reduction of SiO_2 to Si by impurity B, which diffuses into the interface. Over time, mass transfer at the interface reaches a dynamic equilibrium, causing the rate of silicon loss to gradually decrease in Figure 6.

After completing the experiment, off-white substances were found on the wall of the blowing tube near the furnace lid. The silicon melt, when exposed to high temperatures, produced SiO gas, as shown in Eq. [2]. This gas further oxidized to form SiO_2 soot that adhered to the pipe wall. Similar observations were made by other scholars, indicating that during our experiment,

the silicon melt's oxidation caused it to volatilize as a gas, resulting in significant losses along with the formation of slag.

D. Ab Initio Molecular Dynamics Simulation

The geometric structures of Si-B structures doped with O in supercells were obtained by conducting geometry optimization and molecular dynamics simulations at different temperatures, as illustrated in Figure 7. Through these simulations, it is evident that the geometric structures of all systems experienced diverse degrees of modification. To further examine the electronic structures of Si supercells that have been doped with O in the Si-B structure, it is necessary to analyze the bond lengths and bond populations. An effective measure for evaluating bond properties in compounds is the Mulliken overlap population.^[24] In the context of bonding, the term “bond population” generally pertains to the distribution and arrangement of electrons outside the atomic nucleus. The bond populations provide information about the distribution of atoms or molecules at different energy levels. The magnitude of the overlap population can indicate the strength of the bond between atoms, where larger values suggest stronger bonding. To investigate changes in Si-O, Si-B, and B-O bonds in our study, we calculated the bond lengths and populations, which are presented in Table IV.

The geometric structures of the Si-B-O system are presented in Figure 7, both before and after undergoing molecular dynamics (MD) simulations. The results demonstrate significant geometric changes in the system after being subjected to 1 ps of MD simulations at 1723 K, and even more pronounced changes at 1823 K. These observations, when combined with the results of Table IV, indicate a decrease in the population and an increase in the bond lengths of Si-O and Si-B bonds, suggesting a weakening of their interactions following the 1 ps of MD simulations at 1723 K. As the simulation temperature increases to 1823 K, the population of Si-O bonds further decreases, and their bond length increases, indicating a further weakening of the interactions. Additionally, interactions between B-O bonds emerge after 1 ps of MD simulations at both 1723 K and 1823 K. It was also observed that the population of B-O bonds increases from -0.07 to 0.16 , while the bond

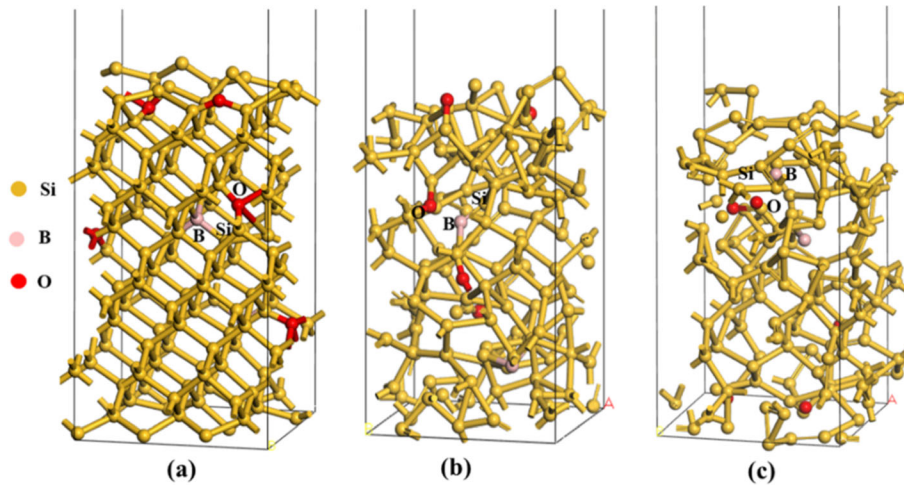


Fig. 7—The structure of the Si-B-O system before and after dynamic simulation is presented as follows: (a) Geometric optimization; (b) Structure obtained after simulating for 1ps at 1723 K; (c) Structure obtained after simulating for 1 ps at 1823 K.

Table IV. Mulliken Population and Bond Length Before and After Dynamics Simulation

Structure	Bond	Structural Optimization		Dynamic Simulation (1723K)		Dynamic Simulation (1823K)	
		Pop.	Len (Å).	Pop.	Len (Å).	Pop.	Len (Å).
Si-B-O	Si-O	0.43	1.685	0.44	1.748	0.44	2.603
	Si-B	0.55	2.101	0.53	2.247	0.16	2.216
	B-O			- 0.07	2.690	0.28	1.666

length decreases from 2.690 to 2.216 Å angstroms with increasing temperature, indicating a strengthening of the interactions between boron and oxygen.

In order to further investigate the impact of O atom doping on the electronic structure and properties of Si-B supercells, calculations were conducted to determine the density of states (DOS) and projected density of states (PDOS). These results are illustrated in Figure 8, where the dashed line corresponds to the Fermi level.

Figure 8 displays the partial density of states (PDOS) for Si-B supercells doped with O, both before and after dynamic simulations. Figure 8(a) represents the PDOS of the optimized Si-B-O system. It is evident that the s orbitals of O predominantly contribute to the total density of states in the range of - 22 to - 19 eV. In the range of - 13 to 3 eV, the PDOS is mainly composed of the p orbitals of O, B, and the s and p orbitals of Si. Figure 8(b) illustrates the PDOS calculated after dynamic simulations at 1723 K. The total density of states between - 23 and - 19 eV is primarily attributed to the s orbitals of O. In the range of - 13 to 3 eV, the combined density of states is predominantly contributed by the p orbitals of O, B, and the s and p orbitals of Si. Figure 8(b) reveals resonating peaks in the density of states for Si, B, and O in the - 13 to 3 eV range, indicating strong interactions among these atoms. Notably, the interaction between Si and B appears to be stronger than that between B and O. Figure 8(c) illustrates the PDOS obtained from dynamic

simulations at a temperature of 1823 K. The s orbitals of O significantly contribute to the total density of states in the - 19 to - 16 eV range, while the p orbitals of O, B, and the s and p orbitals of Si are the primary contributors in the range of - 13 to 13 eV. Overall, the PDOS is shifted towards positive values after dynamic simulations, suggesting an increase in electronic energy and a decrease in system stability. Additionally, a minor peak is observed in the PDOS of B near - 17 eV, which can be attributed to the contribution of the 2p orbitals of O. Within this energy range, the density of states of the 2p orbitals of B and the 2s orbitals of O overlap, indicating sp hybridization and highlighting an enhanced interaction between B and O following the dynamic simulations.

In summary, the results before and after the dynamic simulation indicate that there is a stronger interaction between B and O as the temperature increases, suggesting that oxygen blowing has a certain effect on B removal as well. It was also found that at 1823 K, the interaction between impurity atoms and oxygen atoms is stronger than at 1723 K, indicating that increasing the temperature during the oxygen blowing refining process aids in the removal of impurities. According to Figure 2(a), the content of impurity B decreases with the increase of temperature, which is consistent with the simulation results that increasing temperature helps to remove impurities.

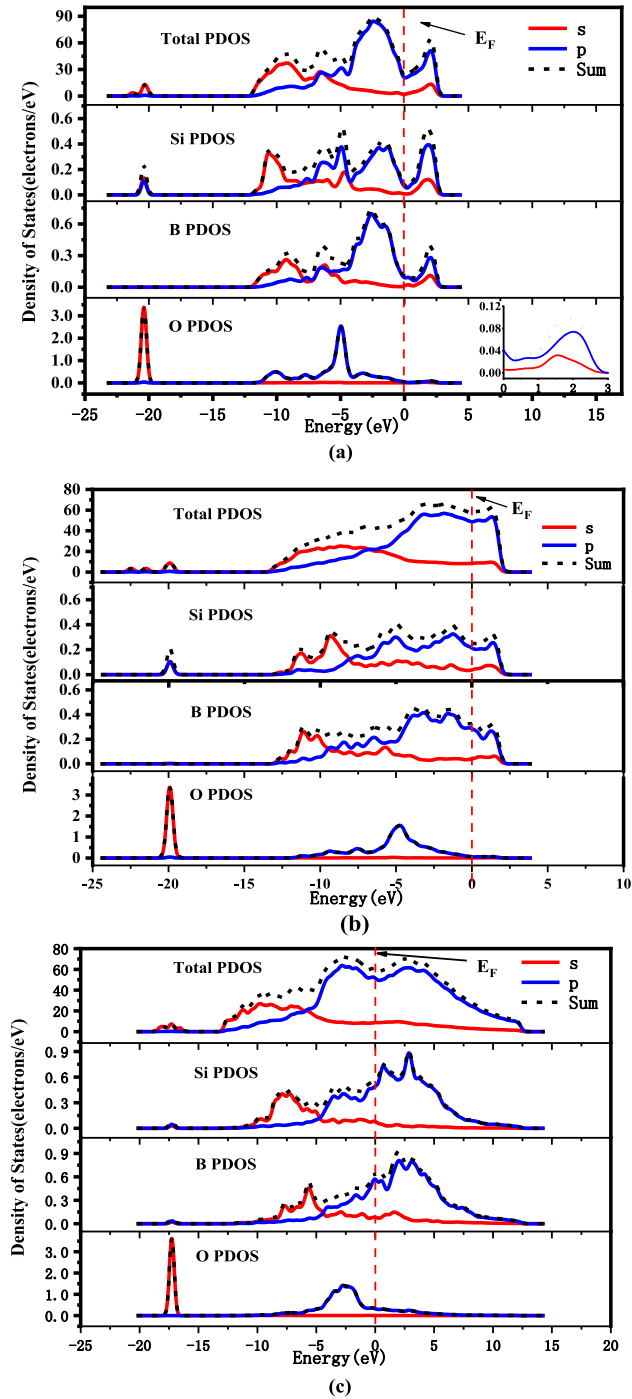


Fig. 8—PDOS before and after Si-B-O system dynamics simulation: (a) Geometric optimization; (b) PDOS simulating 1ps at 1723 K; (c) PDOS simulating 1ps at 1823 K.

E. Diffusion Coefficient of Boron in Silicon Melt

Although the diffusion coefficient of impurities in crystalline silicon has been extensively researched, studying impurity diffusion in silicon melt presents significant experimental challenges due to high temperatures (> 1723 K) and the active chemical reactivity of the melt. As a result, the diffusion coefficient of impurities in silicon melt remains relatively unknown.

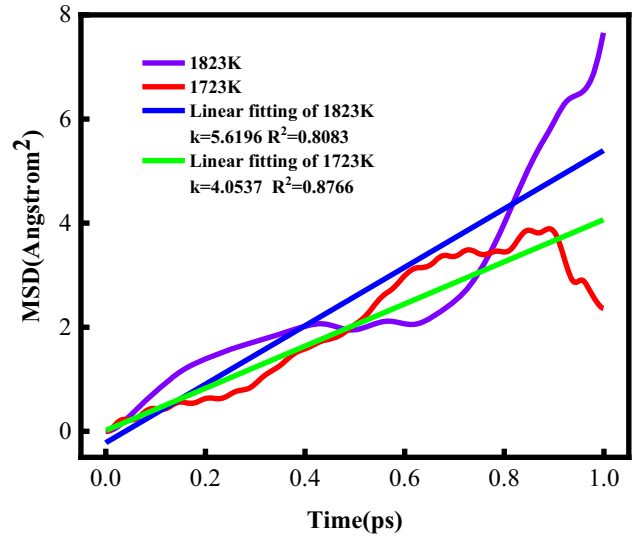


Fig. 9—MSD of boron.

In the absence of experimental data, molecular dynamics methods can be employed to approximate the diffusion coefficients of impurities in silicon melt. This approach provides a reasonable theoretical basis and effectively overcomes experimental difficulties. Diffusion is a process of migration and transfer driven by the thermal motion of particles. During the diffusion process, atoms do not move in a regular manner but instead make irregular jumps between intervals and vacancies. To facilitate the study of diffusion behavior, the Mean Square Displacement (MSD) concept is introduced to describe the motion of particles. The MSD quantifies the net displacement of atoms in the system after multiple jumps. Based on the resulting uniform displacement, the diffusion coefficients of each component in the melt can be determined.

For particles α

$$\langle \Delta r_{\alpha}(t)^2 \rangle = \frac{1}{Z_{\alpha}} \left\langle \sum_{i=1}^{Z_{\alpha}} |r_{\alpha i}(t + t_0) - r_{\alpha i}(t_0)|^2 \right\rangle \quad [7]$$

In the equation, t_0 represents any starting time, and angle brackets represent thermodynamic averages.

According to Einstein's diffusion law:

$$\langle \Delta r_{\alpha}(t)^2 \rangle = 6D_{\alpha}t + A_{\alpha} \quad [8]$$

where D_{α} is the diffusion coefficient of the particle, and the slope of the mean azimuth shift to the time curve is $6 D_{\alpha}$.

A statistical analysis of particle trajectories in silicon melt was performed using MS software to obtain the mean azimuth displacement (MSD) function of boron over time at temperatures of 1723 K and 1823 K. The results are illustrated in Figure 9.

Figure 9 illustrates the increasing trend of the mean square displacement (MSD) of boron impurity in silicon melt as temperature increases. To calculate the diffusion coefficients of various impurity elements, Eq. [8] was utilized in conjunction with the MSD curve. The MSD

curve was fitted, and one-sixth of the slope was determined as the diffusion coefficient of boron in silicon melt. The diffusion coefficients of boron in silicon melt at temperatures of 1723 K and 1823 K were calculated to be 6.756×10^{-9} and $9.366 \times 10^{-9} \text{ m}^2 \text{ s}^{-1}$. The calculations indicate that the diffusion coefficient of impurity boron tends to increase as temperature increases. This observation implies that raising the temperature during the oxygen blowing refining process is beneficial for effective impurity removal.

IV. CONCLUSIONS

At a temperature of 1873 K, oxidative refining has been found to effectively remove non-metallic impurities, such as boron, from industrial silicon. The experimental results demonstrate that with a refining time of 90 minutes, a refining temperature of 1823 K, and an Ar to O₂ gas ratio of 1:1, the content of impurity boron was reduced to 0.0010 pct. Calculations determined the apparent rate constant for the degradation of boron to be $k_B = 5.68 \times 10^{-4} \text{ m s}^{-1}$ and the mass transfer coefficient to be $\beta_B = 1.37 \times 10^{-5} \text{ m s}^{-1}$. During the refining process, silicon oxidized to form silicon dioxide, leading to a loss of silicon. The experimental data shows that as the refining time increases, the rate of silicon loss gradually rises, peaking at 10.12 pct after 90 minutes. Dynamic simulation of the Si–B–O structure revealed a strong interaction between boron and oxygen as the temperature increased. Calculating the mean square displacement of boron atoms, the diffusion coefficients of boron in the silicon melt were determined to be $6.756 \times 10^{-9} \text{ m}^2 \text{ s}^{-1}$ at 1723 K and $9.366 \times 10^{-9} \text{ m}^2 \text{ s}^{-1}$ at 1823 K. These experimental results are consistent with the findings of the simulation analysis, the research presents a theoretical basis for improving the efficiency of the industrial silicon refining process.

ACKNOWLEDGMENTS

The authors wish to acknowledge the financial support on this research from the National Natural Science Foundation of China (22078140), the Talent Training Program of Yunnan of China (202005AC160041), the Key Science and Technology Specific Projects of Yunnan Province (202202AG050012) and the Open Foundation of State Key Laboratory of Complex Nonferrous Metal Resources Clean Utilization (No. CNMRCUKF2205).

COMPETING INTERESTS

The authors declare no competing financial interest.

REFERENCES

1. C. Ballif, F.-J. Haug, M. Boccard, P.J. Verlinden, and G. Hahn: *Nat. Rev. Mater.*, 2022, vol. 7, pp. 597–616.
2. Y. Liu, Y. Li, Y. Wu, G. Yang, L. Mazzarella, P. Procel-Moya, A.C. Tamboli, K. Weber, M. Boccard, O. Isabella, X. Yang, and B. Sun: *Mater. Sci. Eng. R. Rep.*, 2020, vol. 142, 100579.
3. S. Yang, X. Wan, K. Wei, W. Ma, and Z. Wang: *Waste Manag.*, 2021, vol. 120, pp. 820–27.
4. N. He, D. Yang, M. Xu, J. Wu, K. Wei, and W. Ma: *Metall. Mater. Trans. B*, 2021, vol. 52B, pp. 1830–38.
5. Y. Li, W. Chen, J. Lu, X. Lei, and L. Zhang: *J. Electron. Mater.*, 2021, vol. 50, pp. 1386–96.
6. Q. Zhou, J. Wen, J. Wu, W. Ma, M. Xu, K. Wei, Z. Zhang, L. Zhang, and J. Xu: *J. Clean. Prod.*, 2019, vol. 229, pp. 1335–41.
7. S. Thomas, M. Barati, and K. Morita: *JOM*, 2021, vol. 73, pp. 282–92.
8. Y. He, W. Ma, A. Xing, M. Hu, S. Liu, X. Yang, J. Li, S. Du, and W. Zhou: *Mater. Sci. Semicond. Process.*, 2022, vol. 141, 106438.
9. S. Han, N. Tan, K. Wei, and W. Ma: *Sep. Purif. Technol.*, 2022, vol. 280, 119815.
10. A. Hoseinpour, K. Tang, and J. Safarian: *Sep. Purif. Technol.*, 2020, vol. 235, 116284.
11. W. Yu, Y. Xue, J. Mei, X. Zhou, M. Xiong, and S. Zhang: *J. Alloys Compd.*, 2019, vol. 805, pp. 198–204.
12. J. Guo, Y. Liu, L. Liu, J. Liu, J. Kong, S. Wang, S. Jiang, and P. Xing: *Silicon*, 2020, vol. 12, pp. 2405–12.
13. X. Deng, K. Wei, W. Ma, Q. Tang, and H. Zhang: *Trans. Nonferr. Met. Soc. China*, 2023, vol. 33, pp. 1296–1304.
14. J. Wen, X. Deng, K. Wei, and W. Ma: *Silicon*, 2022, vol. 14, pp. 6587–97.
15. Z. Chen and K. Morita: *Metall. Mater. Trans. B*, 2018, vol. 49B, pp. 1205–12.
16. M.S. Islam and M.A. Rhamdhani: *Metall. Mater. Trans. B*, 2018, vol. 49B, pp. 3171–85.
17. J. Li, X. Bai, B. Ban, Q. He, and J. Chen: *Trans. Nonferr. Met. Soc. China*, 2016, vol. 26, pp. 3046–51.
18. W. Jiang, W. Yu, H. Qin, Y. Xue, C. Li, and X. Lv: *Int. J. Hydrog. Energy*, 2019, vol. 44, pp. 13502–08.
19. M.K. Næss, J.E. Olsen, S. Andersson, and G. Tranell: *Oxid. Met.*, 2014, vol. 82, pp. 395–413.
20. Q. He, N. He, D. Yang, J. Wu, K. Wei, and W. Ma: *Metall. Mater. Trans. B*, 2022, vol. 53B, pp. 1841–50.
21. S. Pathirana, E.M.D. Siriwardane, R. Mohottige, D. Çakır, and N. Oncel: *Surf. Sci.*, 2021, vol. 703, 121739.
22. J. Wu, K. Liu, X. Chen, W. Ma, B. Yang, and Y. Dai: *Silicon*, 2015, vol. 7, pp. 253–59.
23. K. Mukai and Z. Yuan: *Mater. Trans. JIM*, 2000, vol. 41, pp. 323–30.
24. S. Aydin: *J. Mater. Sci.*, 2023, vol. 34, p. 771.

Publisher's Note Springer Nature remains neutral with regard to jurisdictional claims in published maps and institutional affiliations.

Springer Nature or its licensor (e.g. a society or other partner) holds exclusive rights to this article under a publishing agreement with the author(s) or other rightsholder(s); author self-archiving of the accepted manuscript version of this article is solely governed by the terms of such publishing agreement and applicable law.